

Cite this: DOI: 10.1039/c0xx00000x

www.rsc.org/xxxxxx

ARTICLE TYPE

Supplementary information

Effect of evaporation on the drop contact angle

A five-microliter solution droplet is deposited onto the device surface, photographed at different times during evaporation by using a Veho VMS-004 digital camera, and then analyzed by the imageJ software to determine the static contact angle. Selected snapshots of the droplet during evaporation are shown in Fig 2.

In Figure S1 we plot the measured contact angle as a function of droplet volume.

Two regions can be clearly distinguished: between 1 μL and 5 μL , the droplet contact angle assumes a constant value of about 146° . This behavior suggests that the receding drop edges wet only the superhydrophobic patterned surface that – in its turn – forces the droplet to assume high contact angles and to preserve its quasi-spherical shape; below 1 μL , and abrupt decrease of the drop contact angle can be observed. In particular, at 0.3 μL a contact angle of $86^\circ \pm 7^\circ$ is measured. This value is consistent with that expected for a flat silanized silicon surface. At this evaporation stage indeed the droplet wets the square-shaped region located in the center of the device pattern. As the evaporation proceeds, the droplet starts to be in contact only with the sensing area of the device. Under this evaporation stage we measure a contact angle

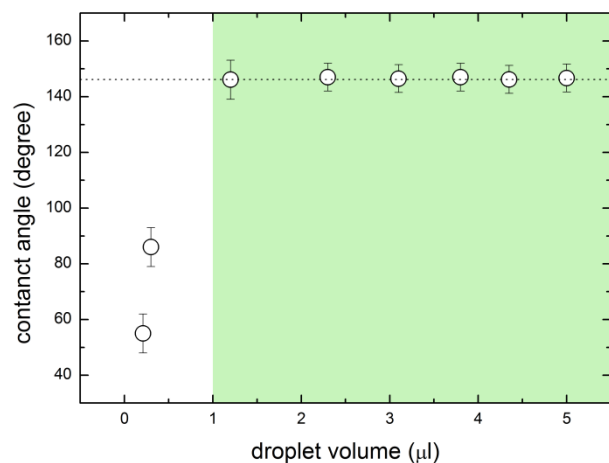


Fig. S1: contact angle evolution during droplet evaporation of $55^\circ \pm 7^\circ$, demonstrating that the overall surface is hydrophilic. Gold nanoantennas cover about 30% of this area, whereas silanized silicon covers the remaining surface. At this evaporation stage, an expected contact angle of 62° can be estimated as a weighted mean of the water contact angle on gold (about 7°) and the measured flat silicon contact angle ($86^\circ \pm 7^\circ$). The expected value is consistent within one standard deviation with the measured one.

Analysis of the secondary structures content of Ferritin.

A 5 μL droplet containing 100 femtomoles of ferritin was deposited on the integrated sensor at room temperature. In figure S2 the amide I absorption band of the ferritin sample after droplet evaporation is reported. The absorption band was computed by assuming a double-transmission geometry through the protein layer through the relation $A = -\log_{10}(R_{\text{sample}}/R_{\text{silicon}})$ derived from the Lambert-Beer's law. Data analysis was performed by using Gaussian curve-fitting procedures together with second derivative (SD) method for the search of the amide components (fig S2). SD procedure was first applied to the amide I band in order to estimate peak frequencies. Each Gaussian component is then assigned to a specific secondary structure of the sample. Frequencies assignment was performed according to

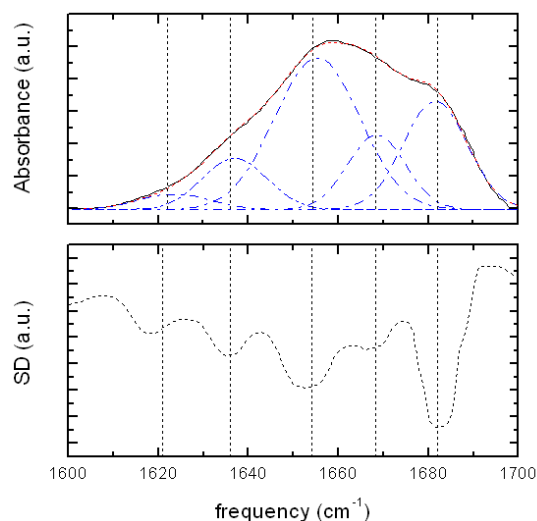
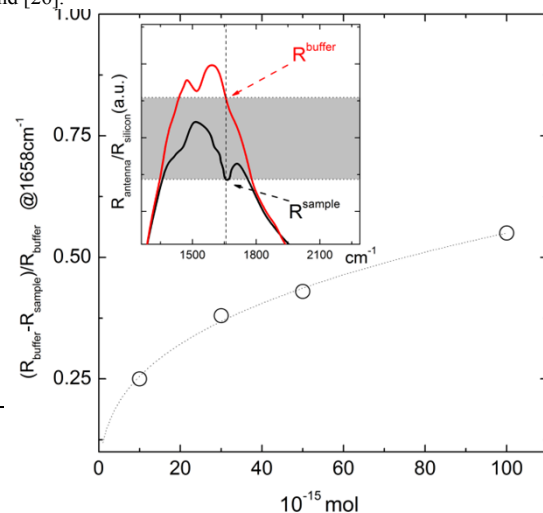


Fig. S2 Upper panel: The amide I absorption spectrum of a droplet containing 100 femtomoles of ferritin (thick line) obtained after droplet evaporation on the superhydrophobic plasmonic sensor is fitted by five separate Gaussian components (dashed blue lines); lower Panel: The second derivative (SD) of the spectrum is reported. Peak frequency assignment was performed according to refs [25] and [26].

ref. [25, 26]. Five Gaussian bands have been resolved for this sample, centered respectively at 1623 cm^{-1} , 1637 cm^{-1} , 1655 cm^{-1} , 1668 cm^{-1} and 1681 cm^{-1} . The ratio between the



integrated intensity of each Gaussian component and that of the whole amide I band provides the relative spectral weight of specific secondary structure of the protein, assuming for them identical values of the molar absorption coefficient. Relative weights, in their turn, may be considered as estimates of the corresponding secondary structures percentage [22]. The estimated secondary structures percentage of the measured sample is summarized in Tab S1.

The most intense component of the amide I absorption spectrum is observed around 1655 cm^{-1} . This spectral component alone accounts for more than 45 % of the total spectral weight and can therefore be associated to the presence of α -helices [23]. An intense peak accounting for about 12% of the band area is detected at 1637 cm^{-1} [23]. This peak can be associated to random structures. In addition to the helix band near 1655 cm^{-1} and to the random coil band near, there are three protein bands around 1623 cm^{-1} , 1668 cm^{-1} and 1681 cm^{-1} . Because apoferritin does not have beta structure in the generally defined sense, the low component at 1623 cm^{-1} may be associated with the short extended chains connecting the helical cylinders [27]. These segments consist in few residues that are not bent into “turns” nor can they form sheet of any kind. The component around 1668 cm^{-1} is usually associated to turns structures in highly helical proteins such as hemoglobin, myoglobin and apoferritin itself. Moreover, apoferritin is reported to have an additional band at 1681 cm^{-1} also probably associated with turns [27].

Therefore, the protein secondary structure content appears to be strongly dominated by helix structures as expected for ferritin, showing that our sensor can provide quantitative information at the femtomole level. Moreover, it is worth stressing that the content of random structures is not higher than that expected (around 10-20% of the total area). These results confirm that the droplet evaporation does not induce major conformational changes in the ferritin sample. Our results are compared to those reported in ref [28] obtained by Circular Dichroism in aqueous solution in the pH range 2.5-10.

Peak (cm^{-1})	1623	1637	1655	1668	1681
Peak assignment	Low component	random structures	α -helix	turns	
Percentage of secondary structures	4%	12%	45%	15%	24%
Percentage obtained by CD Listowsky et al. [28]		11 %	52%	37%	

Tab. S1: (first and second row) estimated secondary structures percentage of the measured apoferritin; (third row) secondary structure content measured by Circular Dichroism in ref [28]

Device sensitivity

The device sensitivity was quantified by measuring the difference between the reflectance at 1658 cm^{-1} of the buffer (R^{buffer}) and that of the sample (R^{sample}), normalized by R^{buffer} . For clarity, these quantities are highlighted in the inset of Fig.S3. In figure S3

we report $(R^{\text{buffer}} - R^{\text{sample}}) / R^{\text{buffer}}$ as a function of the amount of ferritin dissolved in the sample solution expressed in moles.

A slow increase of the $(R^{\text{buffer}} - R^{\text{sample}}) / R^{\text{buffer}}$ ratio can be observed with increasing the initial ferritin molar concentration.

This counterintuitive behavior may depend on the complex interplay between the protein film thickness, which increases with increasing the ferritin amount dissolved in solution, and the electromagnetic field enhancement due to the plasmonic nanoantenna hotspots: the field intensity decreases exponentially with increasing the distance from the device surface, so the sensitivity is higher for thinner films.

Fig S3. Relative variation of the reflectance of the film formed on the nanoantenna array after complete evaporation as a function of the initial molar concentration of protein dispersed in solution before drop evaporation. The buffer sample contains no protein at all. The raw buffer and sample spectra are reported in the inset (therein, the sample contains 50 femtomoles of protein).